Simulation and Measurement of Optical Aberrations of Injection Molded Progressive Addition Lenses

Likai Li[1], Thomas W. Raasch[2], Allen Y. Yi[1]

[1]Department of Integrated Systems Engineering, The Ohio State University, 210 Baker Systems Building, 1971 Neil Ave, Columbus, Ohio 43210, USA

[2]College of Optometry, The Ohio State University, 332 W. 10th Ave, Columbus, Ohio 43210, USA

Abstract

Injection molding is an important mass production tool in optical industry. In this research our aim is to develop a process of combining ultraprecision diamond turning and injection molding to create a unique low cost manufacturing process for progressive addition lenses or PALs. In industry, it is a well-known fact that refractive index variation and geometric deformation of injection molded lenses due to polymers' rheological properties will distort their optical performances. To address this problem, we developed a method of determining the optical aberrations of the injection molded PALs. This method involves reconstructing the wavefront pattern in the presence of uneven refractive index distribution and surface warpage using a finite element method. In addition to numerical modeling, a measurement system based on a Shack-Hartmann wavefront sensor was used to verify the modeling results. The measured spherocylindrical powers and aberrations of the PALs were in good agreement with the model. Consequently, the optical aberrations of injection molded PALs were successfully predicted by

finite element modeling. In summary, it was demonstrated in this study that numerical based optimization for PALs manufacturing is feasible.

1. Introduction

Progressive addition lenses (PALs) have been widely accepted for the compensation of presbyopia (i.e. the decline in ocular accommodation with age) over the past 60 years. Compared with conventional bifocal lenses, PALs provide users a continuous change in spherical optical power through different regions of the lenses. PALs are typically manufactured using casting process. In this process, a monomer is injected into the mold cavity, and then either an initiator is injected, or ultraviolet (UV) exposure is turned on to cure the monomer. However, manufacturing cost for the traditional methods is high due to limited production rate. Therefore, in recently years, new affordable molding techniques have been proposed to produce PALs, such as, glass molding [1] and plastic injection molding [2, 3].

Injection molding process is ideal for high-volume production, and can work with a wide range of materials including optical grade polymer materials. However injection molded optical components have several major issues. These issues include, for example, large geometric shrinkage, refractive index variation and birefringence. Hence, it is of great interest to utilize numerical modeling to investigate and predict the manufacturing process. Kim and Turng used a finite element method (FEM) to model the filling phase of the injection molding process for an optical lens and verified the filling pattern experimentally [4]. Park and Joo applied FEM analysis results of an injection molded lens to a ray tracing simulation [5] and concluded that inhomogeneous distribution of refractive index could occur if molding conditions were not carefully controlled. Besides the simulations for refractive index distribution, Huang [6] and Yang et al. [7] discussed the refractive index variation of injection molded precision optical lenses using different experiments.

Based on the aforementioned research, geometric deformation induced by cooling shrinkage can be minimized in the production of precision optics. In addition, uniform refractive index distribution also plays a crucial role in high quality optical elements. Therefore, in this study we focus on modeling of the injection molding process, including how refractive index variation and geometric deformation are related to wavefront measurements of the molded PALs. Using this approach, the deviation between the design and actual measured optical properties of PALs can be analyzed, predicted and ultimately controlled.

In addition to modeling of wavefront pattern of PALs, comprehensive methods for evaluating and measuring their optical properties have been developed. Castellini et al. modified the Hartmann test to accurately measure the prismatic deviation and spherical power of PALs [8]. Villegas and Artal set up a Shack-Hartmann wavefront sensor system to perform spatially revolved aberration measurement of PALs either isolated or in combination with the eye [9]. Huang compared the wavefront sensing method with a moiré interferometer-based method and a coordinate measuring machine (CMM) method, and discovered that those three methods were comparable for measuring optical powers of PALs [10]. This research utilized a custom optical measurement system based on a Shack-Hartmann wavefront sensor to evaluate second order wavefront aberrations of injection molded PALs, to verify FEM simulated results.

The main objectives of this paper are organized as follows: firstly, perform numerical modeling of the injection molding process to calculate the refractive index variation and geometric deformation. Secondly, fabricate the mold inserts using ultraprecision diamond machining. Thirdly, fabricate PALs by precision injection molding. Finally, measure the wavefront

aberrations of the molded PALs using a custom optical setup. In addition, simulations and measurements of the optical properties of the PALs will be discussed.

2. Simulation of Optical Aberrations

2.1 PAL design

The front convex surface of the PAL in this research is a spherical shape, and its geometry can be described by the radially symmetric second order Zernike term Z_2^0.

$$z = -0.462 \times \sqrt{3} \times (2x^2 + 2y^2 - 1) \quad (1)$$

where z is surface height (mm), *x* and *y* are normalized coordinate positions ranging from -1 to +1, and the nominal radius is 20 mm. The front surface has a peak-valley difference of approximately 1.6 mm and a radius of curvature of 125 mm. Assuming a refractive index of 1.49, this surface has a dioptric power of approximately 3.9 D.

The back concave surface is a freeform surface described by Zernike polynomials

$$z = 0.462 \times \sqrt{3} \times (2x^2 + 2y^2 - 1) - 0.015 \times 2\sqrt{2} \times 3x^2y - y^3 - 0.046 \times 2\sqrt{2}(3x^2y + 3y^3 - 2y) + 0.007 \times 2\sqrt{2}(3x^3 + 3xy^2 - 2x) + 0.007 \times 2\sqrt{2}(x^3 - 3xy^2) + 0.0064 \times 2\sqrt{3}(10x^4y + 20x^2y^3 - 12x^2y + 10y^5 - 12y^3 + 3y) \quad (2)$$

Figure 1 shows the freeform surface of the backside of the PAL where the first polynomial term representing the spherical shape is removed for clarity to show the freeform pattern. The center thickness of the PAL is 2.285 mm.

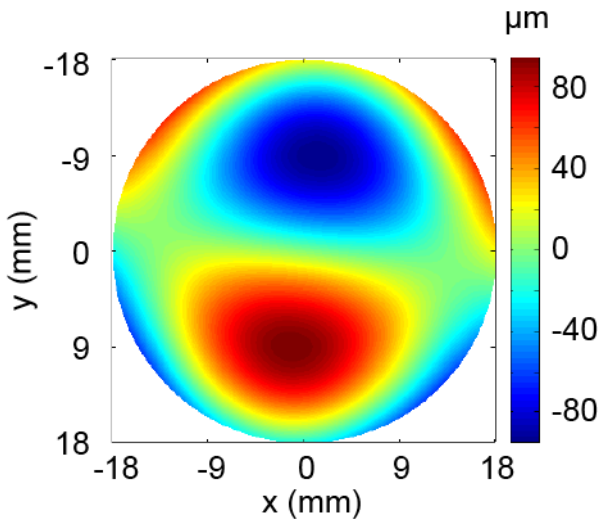

Figure 1. Freeform surface of the backside of the PAL. The first polynomial term was removed to show the freeform geometry.

2.2 Injection molding simulation

After the geometric model was constructed, a true 3D model was generated using HyperMesh (www.altair.com) as shown in Figure 2. The meshed model was then imported to a commercial software package Moldex3D (http://www.moldex3d.com/en/) to complete the FEM simulation. The entire lens model was divided into 12 surface layers of prism elements, and each element layer could be considered as a lens surface. In addition to the lens itself, the mold base and cooling pipes were also included in the model to ensure accuracy but were omitted from Figure 2 for clarity.

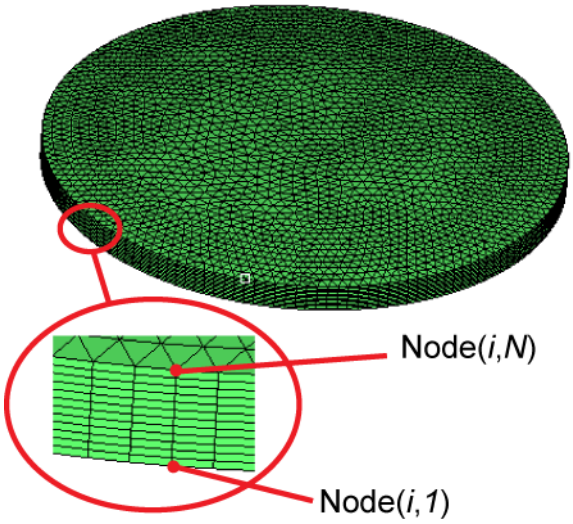

Figure 2. Meshed FEM model. Node(*i*,*1*) is numbered along Number *i* line at the bottom surface of PAL, and Node(*i*,*N*) is the node along Number *i* line at its top surface.

In this simulation, three stages of the injection molding process were analyzed: filling, packing and cooling. An optical grade polymethylmethacrylate (PMMA), trade name, Plexiglas V825, was selected for molding the PALs. The PVT properties of the PMMA are expressed by the modified Tait Model as follows,

$$V = V_0[1 - Cln(1 + P/B)] \tag{3}$$

$$V_0 = \begin{cases} b_{1S} + b_{2S}\bar{T}, if\ T \le T_t \\ b_{1L} + b_{2L}\bar{T}, if\ T > T_t \end{cases} \tag{4}$$

$$B = \begin{cases} b_{3S}\exp(-b_{4S}\bar{T}), if\ T \le T_t \\ b_{3L}\exp(-b_{4L}\bar{T}), if\ T > T_t \end{cases} \tag{5}$$

$$\bar{T} = T - b_5 \tag{6}$$

$$T_t = b_5 + b_6 P \tag{7}$$

where V is specific volume in cm^2, P is pressure in dyne/cm^2, T is temperature in kelvin, and the remaining parameters are constants listed in the left half part of Table 1. The modified Cross WLF model describes the viscosity behavior of this PMMA as the following equations,

$$\eta = \frac{\eta_0}{1+\left(\frac{\eta_0 \gamma}{\gamma^*}\right)^{1-n}} \quad (8)$$

$$\eta_0 = Bexp\left(\frac{T_b}{T}\right) \quad (9)$$

where η is viscosity in g/cm s, γ is shear rate in dyne/cm^2, and the remaining parameters are shown in the right half of Table 1. These material properties were directly taken from the Moldex3D database. Additionally, Table 2 also summarizes the values of the molding condition used in this work.

Table 1. Material parameters of PMMA.

PVT Tait Model		**Viscosity Cross WLF Model**	
Parameters	**Values**	**Parameters**	**Values**
b_{1L} (cc/g)	0.85982	n	0.21
b_{1S} (cc/g)	0.860702	γ^* (dyne/cm^2)	1.48×10^6
b_{2L} (cc/g k)	0.0005697	B (g/cm s)	1×10^{-16}
b_{2S} (cc/g k)	0.0001995	T_b (K)	24294
b_{3L} (dyne/cm^2)	2.09×10^9		
b_{3S} (dyne/cm^2)	2.73×10^9		
b_{4L} (1/K)	0.0049083		

b_{4s} (1/K)	0.003394		
b_5 (K)	383		
b_6 (cm^2 K/dyne)	2×10^{-8}		
C	0.0894		

Table 2. Injection molding condition.

Molding parameters	**Values**
Melt temperature (℃)	250
Mold temperature (℃)	75
Injection velocity (mm/s)	200
Maximum injection pressure (MPa)	100
Velocity/pressure switch (vol %)	90
Packing pressure (MPa)	80
Packing time (s)	6
Cooling time (s)	25
Coolant temperature (℃)	65

As mentioned previously, the computed geometric deformation and refractive index distribution were exported from the FEM calculation for later discussion. The geometric deformation primarily has an impact on optical refraction, so the nodes' positions on the top and bottom surface meshes were extracted for numerical analysis of its optical aberration in next section. Furthermore, uneven cooling as well as the polymer's rheological properties could result in an

unevenly distributed density that consequently causes variation in refractive index [7]. Therefore refractive index information at each node was also collected for optical aberration analysis. It should be noted here that birefringence is defined as a variation in refractive index with polarization angle at any point inside the lens. Refractive index in this study is considered to be a scalar, which can vary with lens location.

2.3 Optical aberration calculation

The refractive index variation on the *xy* plane was calculated by averaging refractive index values of all nodes along one line in the thickness direction of the PAL, or

$$n_i = \left(\sum_{j=1}^{N} n(i,j)\right)/N, \tag{10}$$

where n_i is the averaged refractive index value along the Number i line in the thickness direction, $n(i, j)$ is the refractive index of the j^{th} node on the Number i line or Node(i, j), N is the number of the nodes on the Number i line. Figure 2 illustrates the numbering map. Hence, the refractive index variation could be obtained by

$$\Delta n_i = n_i - \sum_{j=1}^{N_A} n_j/N_A, \tag{11}$$

where N_A is the number of the lines along the thickness direction in the mesh model.

As for the surface warpage, in this study it was defined as the geometric deformation in lens thickness. For example, the thickness between top and bottom surface along the Number i line was calculated using the following equation,

$$d_i' = z'(i,N) - z'(i,1), \tag{12}$$

where $z'(i, 1)$ and $z'(i, N)$ are z coordinate positions of Node (i, j) on the fitted bottom deformed surface and Node (i,N) on the fitted top deformed surfaces, respectively. Therefore, the optical path difference (OPD) when both inhomogeneous refractive index and geometric deformation were considered could be calculated by,

$$D = (\Delta n_i + n_0 - 1) \times (d_i' - t_0), \quad (13)$$

where n_0 is the nominal refractive index of the selected PMMA, which is 1.49, t_0 is the center thickness of the PAL, which is 2.285 mm in this study.

The calculated OPD was fitted to a Zernike polynomial up through the 8th order, or 45 terms using a least square method. The Zernike coefficients of the 45 terms were annotated as a column vector *cc*. Moreover, if a subaperture was translated within the original aperture of the lens, the Zernike coefficient vector for the newly translated subaperture could be calculated by the following equation

$$cc' = TZ \times ((ZT(x, y) \times cc).* rs_j), \quad (14)$$

where, cc' is transformed Zernike coefficient vector, TZ and $ZT(x,y)$ are Taylor-to-Zernike and Zernike-to-Taylor transformation matrices respectively, rs_j is a column vector of size rescaling terms, and '.*' represents element-by-element multiplication. The detailed explanation of this method for calculating transformed Zernike coefficients can be found in [11]. In this way, the spherocylindrical power with this subaperture could be obtained according to the second order Zernike polynomial coefficients:

$$M = \frac{-c_2^0 4\sqrt{3}}{r^2}, \quad (15)$$

$$J_0 = \frac{-c_2^2 2\sqrt{6}}{r^2}, \quad (16)$$

$$J_{45} = \frac{-c_2^{-2} 2\sqrt{6}}{r^2}, \quad (17)$$

where M, J_0, J_{45}, in units of diopters, are spherical defocus, orthogonal astigmatism and oblique astigmatism, respectively [12]. In Equations 15~17, these second order Zernike coefficients c_2^m have meridional frequency m, and have units of μm. The radius of the subaperture, r, has units of mm. Finally, the calculated spherocylindrical powers of all the arrayed subapertures or pupils are assembled in their corresponding positions to plot the figures of the optical powers for the entire PAL.

3. Fabrications and Measurements

3.1. Mold machining and PAL injection molding

For the mold fabrication process, the mold insert with the convex freeform surface was machined on the Freeform Generator 350 (Moore Nanotechnology, Inc., Keene, New Hampshire) using ultraprecision diamond slow tool servo to optical quality. More information of the slow tool servo technique can be found elsewhere [13]. In this study, a diamond tool with a controlled radius 2.6055 mm was utilized. The tool path trajectory was compensated offline by the tool radius. On the finishing machining path for the convex freeform optical surface, the cutting depth was 5 μm and the feedrate was 20 mm/min. 6061 aluminum alloy was used as the material of the mold inserts. Figure 3 shows the finished aluminum mold inserts for the PAL. The surface roughness of the convex surface was approximately 10 nm measured using the Wyko NT9100 optical profilometer. The concave spherical mold surface was machined by conventional

ultraprecision diamond turning and its surface roughness was measured to be about 8 nm. No post-polishing was performed on the inserts.

Figure 3. Finished ultraprecision diamond turned mold inserts for PAL injection molding.

The diamond turned mold inserts were then installed in the microinjection molding machine (LD30EH2, Sodick Plustech) for molding test. The microinjection molding machine employed in this study can generate up to 250 mm/s maximum injection velocity with a 30 ton maximum clamping force. The special injection system of this machine has separated screw plasticizing unit and plunger injection unit to precisely manage the micro feature replication by their independent controls. Same as the material modeled in the simulation, the optical grade PMMA, Plexiglas V825, was used in the experiment. The experimental molding conditions were the same as in the simulations listed in Table 2. The injection molded PALs are shown in Figure 4.

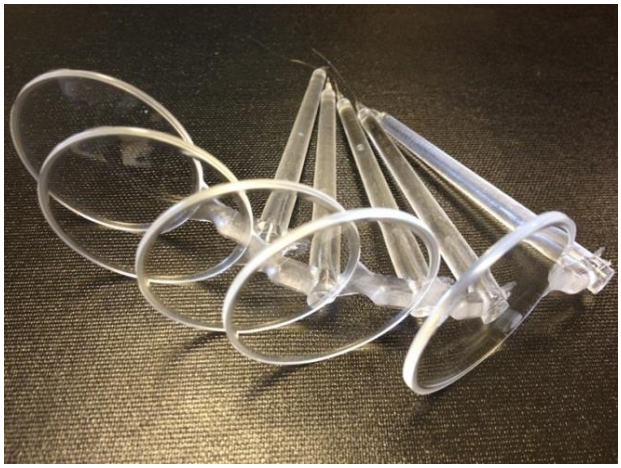

Figure 4. PALs manufactured by microinjection molding.

3.2 Optical measurements

Figure 5 shows a schematic of the wavefront sensor measuring system. A small, distant white light source produces a nearly flat wavefront in the plane of the tested PAL. The refracted wavefront traverses two relay lenses, and arrives at the Shack-Hartmann sensor. The two relay lenses (elements 3 and 4 in Figure 5) are positioned such that the PAL and the microlens array are in optically conjugate planes. To position any given location of the PAL along the measurement axis, the lens is pivoted around horizontal and vertical axes, the intersection of which represents the center of rotation of an eye 27 mm behind the lens. Lens positioning is performed with stepper-motors that pivot the lens mount around the horizontal and vertical rotation axes.

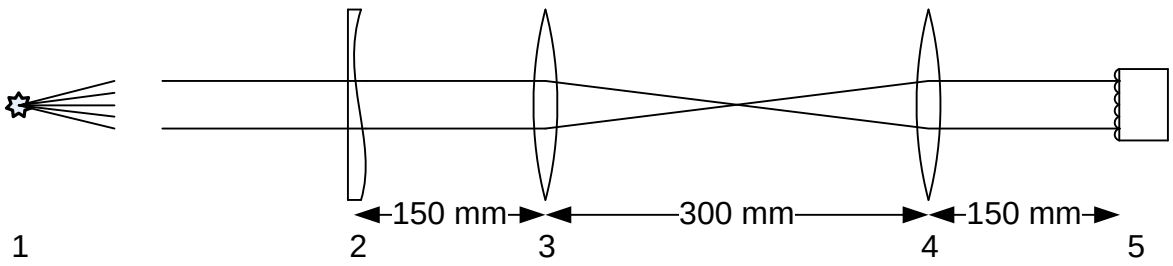

Figure 5. Schematic of the wavefront measuring system. 1: Distant source; 2: PAL; 3 and 4: 150 mm fl lenses; 5: Shack-Hartmann sensor.

The Shack-Hartmann sensor consists of a microlens array and a CCD camera. A 3.5 mm virtual stop is placed at the microlens array, and since it is conjugate with the lens plane at unit magnification, represents a 3.5 mm eye pupil viewing through that lens position. Each microlens is 0.36 mm on a side, and with a 3.5 mm diameter pupil, approximately 70 lenslet spot images are contained in the camera image. When a wavefront enters the sensor, it is partitioned by the microlens array. The local tilt of the wavefront within each subaperture causes a displacement of the focal spot from the reference central position. Thus, these deviations can be assembled to reconstruct the wavefront variation [14]. Wavefront aberration arises from the freeform nature of the PAL, the non-uniform refractive index distribution, and geometric deformation of the lens surfaces.

4. Results and Discussion

As discussed in Section 2, the rheological phenomenon and uneven cooling lead to the refractive index variation of the injection molded PAL. The FEM results show that the refractive index on one surface layer varies in the scale of 10^{-4}, whereas the variation scale among the multiple surface layers along the thickness direction is 10^{-3}. Figure 6 illustrates the refractive index variation of the molded PAL calculated by Equation 11. The location of the injection gate is at the bottom of this picture. Although the upper limit of the injection pressure was set as 100 MPa, the actual maximum injection pressure was about 80 MPa indicated by the FEM simulation which was almost equal to the packing pressure. This is an effective packing with high packing pressure and long packing time. Thus, compared with previous studies [5, 7], the distribution

variation is relatively small with a maximum deviation of 6×10^{-4}. In addition to the small deviation, because higher packing pressure occurs closer to the injection gate, the general trend of the distribution decreases along the flow direction.

Despite of the dominant effects by the sufficient packing, the uneven cooling may outweigh the packing effects. For example, the material at the region farther away from the center in the radial direction cools and shrinks faster than the central region. This causes denser material formation resulting in a higher refractive index. More specifically, as an example, some region at the top may have higher refractive index than the lower part although the top region is farther away from the injection gate. Additionally, since a thinner area cools faster than a thicker area, this analysis can also apply to the thinner top region when compared with the thicker bottom. In Figure 6, the index variation is similar to the freeform geometry pattern illustrated in Figure 1, which suggests that regional thickness discrepancies may be more important than radial position differences for refractive index variation in terms of thermal transportation. So, with all of these effects combined, the highest refractive index happens at the bottom half of the PAL surrounded by an ox-horn-shaped transition region from the bottom to the top.

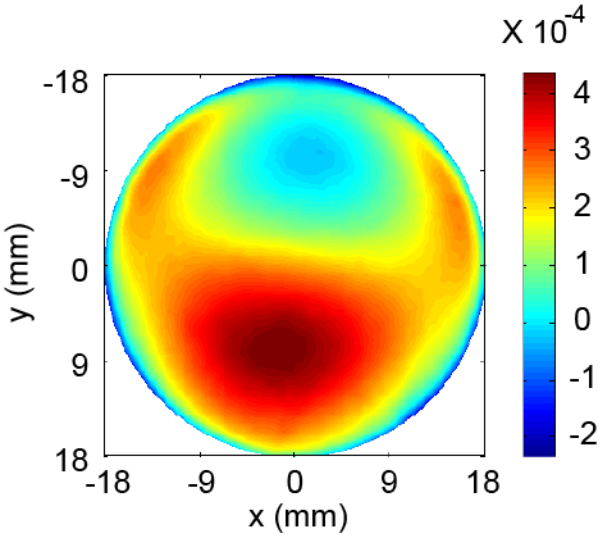

Figure 6. Simulated refractive index variation of an injection molded PAL.

Geometric deformation is another important factor that influences the PAL's optical performance. As defined before, the geometric deformation is the thickness deviation between the design and the molded parts. The simulated thickness for the molded lens between the top and bottom surfaces can be calculated by Equation 12. If similar derivations are applied to the original design, the thickness deviation is the discrepancy between the design and simulation. Figure 7 shows the simulated thickness deviation between the design and the molded PAL. As seen in this figure, the thicker bottom part of the PAL has more shrinkage in thickness, although it is closer to the injection gate or the highest packing pressure location. Consistent with the analysis above, the larger shrinkage at the thicker region may also result in higher refractive index. In this situation, the regional thickness difference largely contributes to the thickness change of the molded PAL.

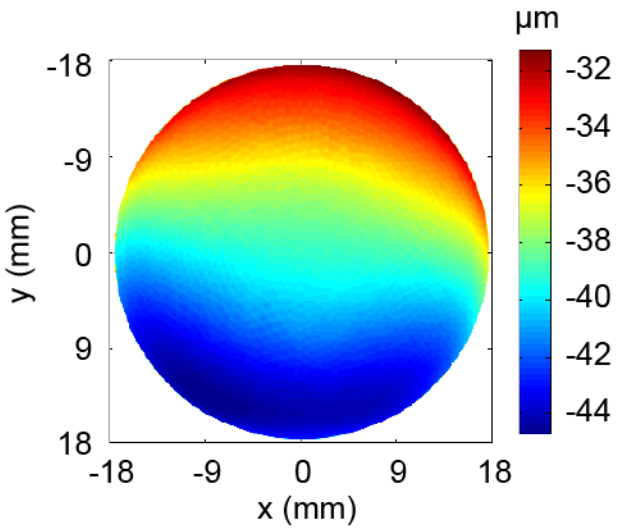

Figure 7. Simulated thickness change over *xy* plane of PAL.

Considering both the refractive index variation and geometric deformation, each component of the optical aberrations of the injection molded PAL can be determined by the derivations developed in Section 2.3. Figures 8 ~ 10 show the PAL's spherical power M, and the two cylindrical components J_0 and J_{45} respectively, in terms of the design, simulation and measurement results. It can be seen that the variation scales of the simulated optical powers and aberrations are slightly larger than the design.

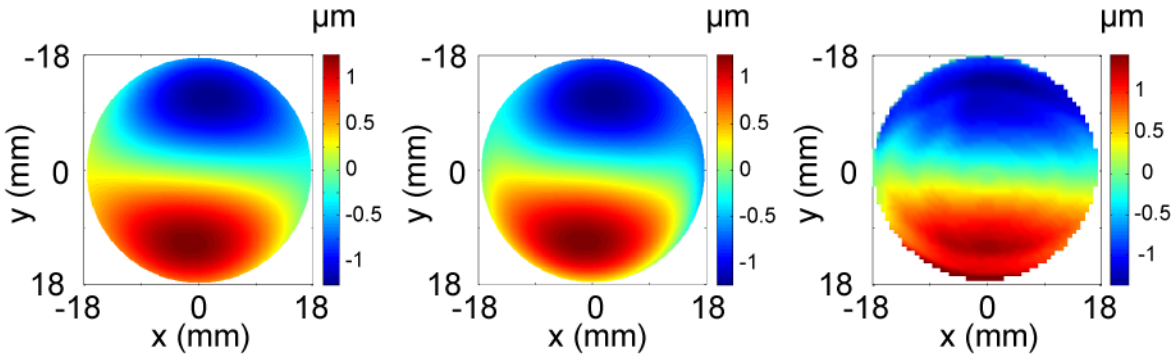

(a) (b) (c)

Figure 8. Spherical power M of molded PAL (a) design (b) simulation (c) measurement

Figure 8b shows that the magnitude of the simulation is smaller than the design. In addition the optical aberration patterns were also slightly changed when the injection molding process was taken into consideration. For instance, as the simulated spherical power in Figure 8(b), a round corner appears at the left side of the bottom red area in contrast to the flat slope at the transition area between red and yellow region in Figure 8(a). There is a falling tip pattern on the right side of the blue area though smooth progression in design. Additionally, as can be observed in Figure 9(b), the top area in the red zone is larger than the blue area at the bottom while the overall pattern is rotational symmetric in the original design as shown in Figure 9(a). Moreover, the

simulated cylindrical aberration component J_{45} in Figure 10(b) displays the sagging blue area and red area, but these two areas are symmetric about the horizontal direction in the design as illustrated in Figure 10(a). Finally, the Shack-Hartmann measurements (8c, 9c, 10c), appear to be in relatively good agreement with the simulations.

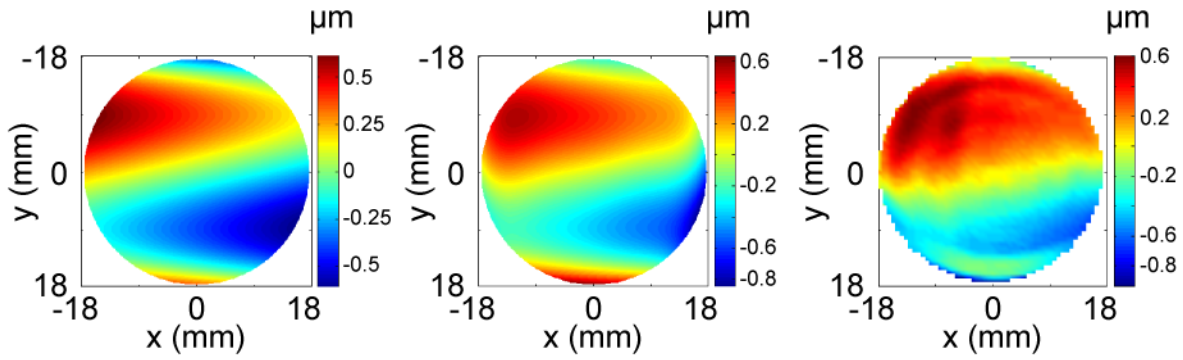

(a) (b) (c)

Figure 9. Cylindrical component J_0 of injection molded PAL (a) design (b) simulation (c) measurement

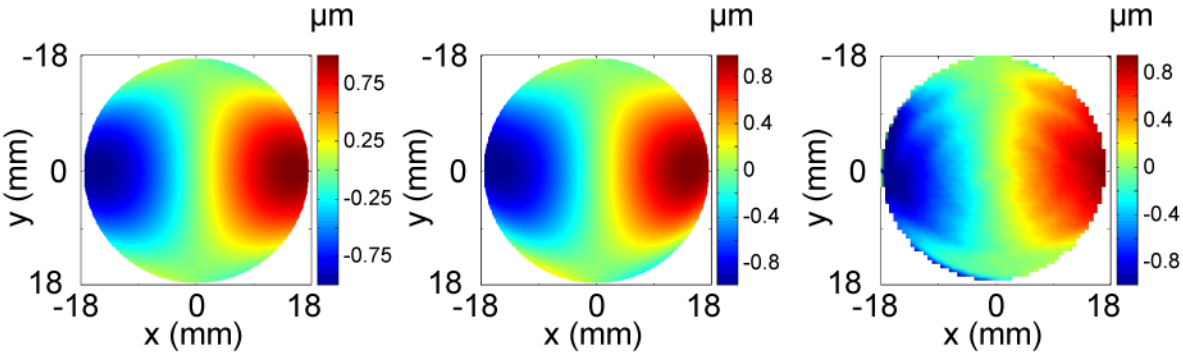

(a) (b) (c)

Figure 10. Comparison of (a) designed, (b) simulated and (c) measured cylindrical component J_{45} of injection molded PAL.

There are many other possible reasons that can potentially affect the accuracy of the evaluation process. For example, in ophthalmic applications, the distance between the lens and the entrance pupil of the eye is typically about 15 mm. The wavefront will, in general, change shape as it travels that distance. However, in this instance, curvatures are not high enough for this difference to be clinically meaningful. In addition, meshing strategies, materials models and boundary conditions also have an influence on the final simulated results. Furthermore, in the optical measurement apparatus, the PAL was rotated around an ocular center of rotation 27 mm behind the lens to select each measurement area. This was done to imitate a rotating eye as it views through different locations on the lens. Nevertheless, large oblique incidence will affect wavefront shape, which is not yet accounted for in this modeling. Finally, precision of centering and positioning the PAL could be improved.

In this research, the goal was to search for a preferred injection molding condition for the PALs. Specifically, packing pressure, packing time, and injection time, were investigated. Two levels of each parameter were investigated, as listed in Table 3. Our conclusions can be summarized as: (a) neither the packing time nor the injection time has a significant impact on the optical properties of the PALs, (b) higher packing pressure results in smaller refractive index variation and smaller thickness change (refractive index variation $-1.5\times10^{-4} \sim 3.5\times10^{-4}$, thickness change -15.5 ~ -11 μm), (c) the patterns and the scales of the second order optical powers and aberrations do not change dramatically when the injection molding process conditions are varied.

Table 3. Injection molding conditions for design of experiment.

Process	**Packing pressure**	**Packing**	**Injection**

number	(Kg/cm^2)	**time** (s)	**time** (s)
1	800	3	0.125
2	1,200	3	0.125
3	1,200	6	0.125
4	800	6	0.125
5	800	3	0.1
6	800	6	0.1
7	1,200	3	0.1
8	1,200	6	0.1

The first conclusion can be explained by the fact that packing times were adequate to offset shrinkage. Furthermore, the higher packing pressure reduced the absolute amount of thickness deformation. However, deformation patterns plotted in the same way as Figure 7 were still quite similar between the two packing pressures. From the test conditions, the No. 2 process was adopted for future production of PALs because of its shorter cycle time, less power required, more uniform refractive index distribution and less geometric deformation.

5. Conclusions

Transparent polymers are of considerable significance in today's optical industry for their intrinsic advantages in mass production over traditional glass materials. This research presents a new approach to fabricate PALs using the combination of ultraprecision diamond turning and precision injection molding. This approach has wide industrialization potential due to its affordability. Also, it is demonstrated that the modeling of the injection molded PALs can be

used to successfully predict their optical aberrations. The numerical modeling can also be utilized to optimize manufacturing processes.

Results of refractive index variation and geometric deformation of the injection molded PALs from finite element modeling were used to calculate properties of the wavefront refracted through the lens. Furthermore, we identified an optimal manufacturing process condition from the range of conditions explored here. We varied the packing pressure, packing time and injection time. One molding condition was selected for reduced cycle time, economic power requirement, uniform refractive index distribution and accurate geometry replication.

Future work would include: (a) compensating for refractive index variation and geometric deformation in the mold surface design, (b) incorporating wavefront propagation calculation into the optical modeling, (c) improving positioning accuracy of PALs in Shack-Hartmann wavefront sensing system. Future work may also include examination of other lens materials, such as hybrid glass-polymers, to improve optical quality [15, 16].

Acknowledgement

This study was partially based on the work supported by National Science Foundation under Grant Numbers CMMI-0928521 and EEC-0914790. Any opinions, findings, and conclusions or recommendations expressed in this material are those of the authors and do not necessarily reflect the views of the National Science Foundation.

References

[1] Lochegnies, D., Moreau, P., Hanriot, F., & Hugonneaux, P. (2013). 3D modelling of thermal replication for designing progressive glass moulds. New Journal of Glass and Ceramics, 3, 34-42.

[2] Hsu, W.-Y., Liu, Y.-L., Cheng, Y.-C., & Su, G.-D. (2010, October). Design and fabrication of the progressive addition lens. In Frontiers in Optics. Optical Society of America.

[3] Cheung, C. F., Kong, L. B., Ho, L. T., To, S., Wang, B., & Lai, K. T. (2012). An integrated approach for design, ultra-precision polishing and measurement of freeform progressive lenses. In 6th International Symposium on Advanced Optical Manufacturing and Testing Technologies (AOMATT 2012) (pp. 84160C-84160C). International Society for Optics and Photonics.

[4] Kim, S.-W., & Turng, L.-S. (2006). Three-dimensional numerical simulation of injection molding filling of optical lens and multiscale geometry using finite element method. Polymer Engineering & Science, 46(9), 1263-1274.

[5] Park, K., & Joo, W. (2008). Numerical evaluation of a plastic lens by coupling injection molding analysis with optical simulation. Japanese Journal of Applied Physics, 47, 8402-8407.

[6] Huang, C. (2008). Investigation of injection molding process for high precision polymer lens manufacturing (Doctoral dissertation, The Ohio State University).

[7] Yang, C., Su, L., Huang, C., Huang, H.-X., Castro, J. M., & Yi, A. Y. (2011). Effect of packing pressure on refractive index variation in injection molding of precision plastic optical lens. Advances in Polymer Technology, 30(1), 51-61.

[8] Castellini, C., Francini, F., & Tiribilli, B. (1994). Hartmann test modification for measuring ophthalmic progressive lenses. Applied Optics, 33(19), 4120-4124.

[9] Villegas, E. A., & Artal, P. (2003). Spatially resolved wavefront aberrations of ophthalmic progressive-power lenses in normal viewing conditions. Optometry & Vision Science, 80(2), 106-114.

[10] Huang, C.-Y., Raasch, T. W., Yi, A. Y., Sheedy, J. E., Andre, B., & Bullimore, M. A. (2012). Comparison of three techniques in measuring progressive addition lenses. Optometry & Vision Science, 89(11), 1564-1573.

[11] Raasch, T. (2011). Aberrations and spherocylindrical powers within subapertures of freeform surfaces. JOSA A, 28(12), 2642-2646.

[12] Thibos, L. N., Hong, X., Bradley, A., & Applegate, R. A. (2004). Accuracy and precision of objective refraction from wavefront aberrations. Journal of Vision, 4(4).

[13] Yi, A. Y., & Li, L. (2005). Design and fabrication of a microlens array by use of a slow tool servo. Optics letters, 30(13), 1707-1709.

[14] Shack, R. V., & Platt, B. C. (1971). Production and use of a lenticular Hartmann screen. JOSA, 61(5), 656.

[15] Li, L., He, P., Wang, F., Georgiadis, K., Dambon, O., Klocke, F., & Yi, A. Y. (2011). A hybrid polymer–glass achromatic microlens array fabricated by compression molding. Journal of Optics, 13(5), 055407.

[16] Li, L., & Yi, A. Y. (2013). Design and manufacturing of an affordable injection molded precision hybrid glass-polymer achromatic lens. In Annual Technical Conference (ANTEC). Society of Plastics Engineers.